Enhancing Microinverter Energy Capture With Submodule Differential Power Processing

Shibin Qin, *Student Member, IEEE*, Christopher B. Barth, *Student Member, IEEE*, and Robert C. N. Pilawa-Podgurski, *Member, IEEE*

***Abstract*—Differential power processing (DPP) is a power electronics system architecture that configures dc–dc converters in parallel with the PV string to improve its power yield. The parallel nature of the DPP architecture brings a number of benefits, such as low converter power rating and low power losses, all of which make DPP especially suitable for submodule-level maximum power point tracking (MPPT). Meanwhile, microinverters typically perform only module-level MPPT and do not address power losses due to uncompensated submodule mismatch. In this paper, we introduce DPP converters into a microinverter system to improve its energy capture by recovering power losses due to submodule mismatch. The control method to interface DPP converters with a microinverter for submodule MPPT is presented and the tradeoff between tracking accuracy and control overhead is analyzed. A small-footprint DPP converter is designed. A digitally assisted windowed sensing technique is also implemented to address the challenge of precise current sensing. Altogether, the proposed solution seamlessly integrates DPP into the existing microinverter design. To demonstrate the effectiveness of the proposed solution, a hardware prototype has been built and tested with an off-the-shelf commercial microinverter. The improvement in energy capture with DPP converters has been experimentally verified.**

***Index Terms*—Differential power processing, maximum power point trackers, micro-inverter, photovoltaic, power systems, power converters.**

I. Introduction

In photovoltaic energy systems, PV elements (cells, submodules, and modules) are often connected in series at every level for increased voltage and minimal wiring. Typically, each PV module consists of three series-connected submodules, each with a bypass diode connected in parallel, and each submodule consists of 20–24 PV cells. Due to various causes, such as partial shading, manufacturing variability, thermal gradients, nonuniform aging, etc., series-connected PV elements often have mismatched *I–V* characteristics. Since all elements connected in series share the same current, some PV elements cannot operate at their individual maximum power point, and the power output of the entire string is limited by the underperforming elements. The bypass diode in parallel with each submodule can mitigate this mismatch to some extent and prevent PV hot spotting [1], [2], but the power loss can still be significant when severe mismatch exists between PV submodules.

To fully recover the power loss due to PV module-level mismatch, distributed power electronics, such as dc optimizers [see Fig. 1(a)] [3]–[5] and microinverters [see Fig. 1(b)] [6]–[8] have been proposed to overcome the mismatch problem by performing module-level MPPT. Compared to a PV string with only a central inverter, these two solutions can improve the power yield by mitigating the mismatch between PV modules. However, the mismatch between submodules within one PV module is still not compensated for. A submodule-level dc optimizer has been proposed [9], but microinverters typically work only at the module level. Submodule-level microinverters are not practical today due to the high hardware cost and relatively low efficiency associated with the large voltage step-up required.

In search of submodule MPPT solutions, the differential power processing (DPP) architecture [see Fig. 1(c)] has been shown to be a viable alternative. Such structure has been explored in the previous literature in battery management [10], [11], data center power distribution [12]–[14], multicore CPU power delivery [15]–[18], etc., as well as in photovoltaic applications [19]–[39]. A high-level introduction to the DPP concept in photovoltaic applications can be found in [40]. In the DPP architecture, the bulk power common to all PV elements flows through the series connection without any intermediate conversion, while the DPP converters manage the differential power between adjacent PV elements to balance the mismatch (without the conduction of bypass diodes). With proper control, DPP converters can fine-tune the voltage of PV elements and perform MPPT [28]. Since the DPP converters only process the power mismatch, which is typically only a fraction of the full power, they can be rated at a relatively low power level, resulting in a small-size low-cost hardware implementation. Moreover, each DPP converter is processing much less power than a dc submodule optimizer on average. Given similar converter efficiencies, the overall power loss of a DPP architecture is thus significantly smaller. When there is only a very small mismatch or no mismatch existing between PV submodules, the parallel nature of the DPP architecture allows the converters to be turned OFF, while the dc optimizers always have to process the full power even when there is no mismatch. In other words, the system efficiency of a dc optimizer system is fundamentally limited by the dc–dc converters, while the DPP system decouples the system efficiency from the dc–dc converter efficiency.

To better illustrate the efficiency comparison between the dc optimizer and DPP system, Fig. 2 provides a numerical example where one PV module (three submodules) is affected by a small mismatch—the three PV submodules have a 100%, 90%, and

Manuscript received November 22, 2014; revised March 12, 2015 and June 1, 2015; accepted July 18, 2015. Date of publication August 4, 2015; date of current version December 10, 2015. This work was supported in part by the Advanced Research Projects Agency-Energy, U.S. Department of Energy, under Award DE-AR0000217. Recommended for publication by Associate Editor V. Agarwal.

The authors are with the Department of Electrical and Computer Engineering, University of Illinois at Urbana-Champaign, Urbana, IL 61801 USA (e-mail: sqin3@illinois.edu; cbarth2@illinois.edu; pilawa@illinois.edu).

Color versions of one or more of the figures in this paper are available online at http://ieeexplore.ieee.org.

Digital Object Identifier 10.1109/TPEL.2015.2464235

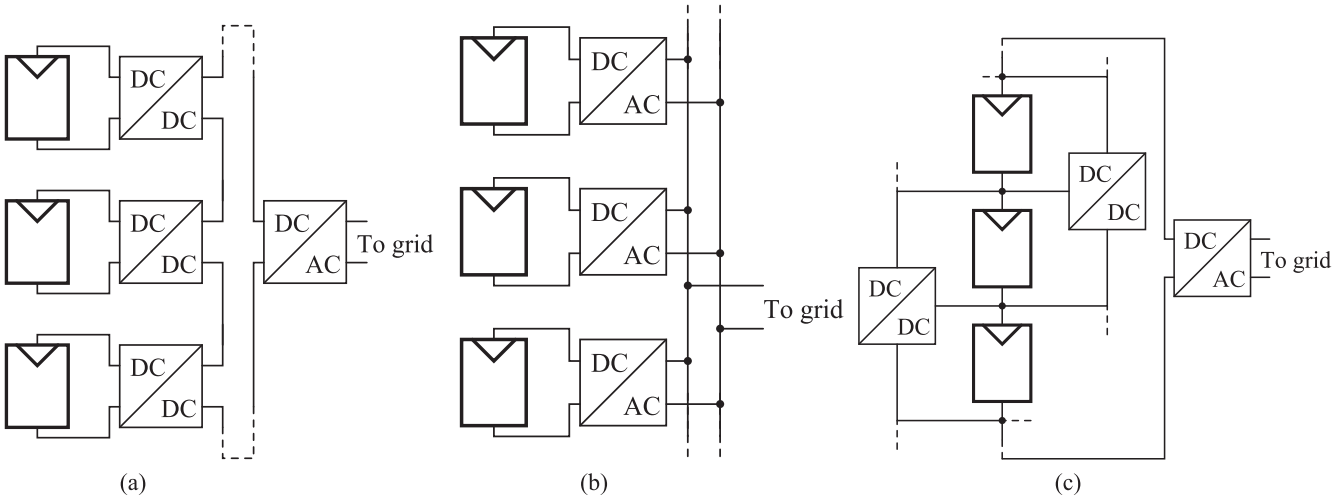

Fig. 1. Three types of distributed power electronics solutions for PV systems. (a) DC optimizer. (b) Microinverter. (c) DPP-based system.

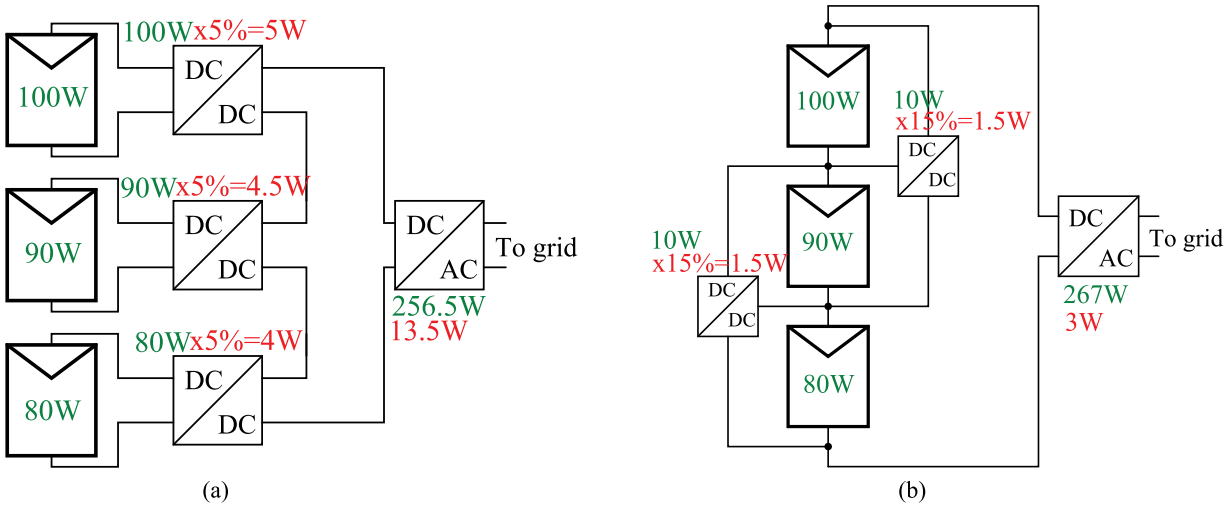

Fig. 2. Comparison of dc stage efficiency between dc optimizer system and DPP system. (a) DC optimizer. (b) DPP.

TABLE I
COMPARISON OF DC STAGE EFFICIENCY FOR THE EXAMPLE IN FIG. 2

Device	dc optimizer	DPP
Total PV Submodule Power [W]	270	270
Total Power Processed [W]	270	20
Average Converter Efficiency [%]	95%	85%
Power Loss in dc Stage [W]	13.5	3
dc Stage Efficiency [%]	95%	98.9%

80% normalized irradiance, respectively. Either dc optimizer or DPP converters can be applied to perform submodule MPPT to mitigate the mismatch. The analysis of the *dc stage efficiencies* of both systems are summarized in Table I. Note that since the dc optimizers are expected to operate mostly in a full load condition while the DPP converters are expected to operate in a light load condition, we assume a higher converter efficiency for the dc optimizers than that for the DPP converters. Even so, the overall dc stage efficiency of the DPP system is significantly higher as presented in Table I. A more detailed and more general example can be found in [28].

Due to the aforementioned advantages, submodule-level DPP has been widely proposed to be applied directly to utility-scale PV arrays [19]–[24], [26]–[28], [34], [41], [42] or merged with module-level dc optimizers [25], [30] or microinverters [39]. However, most of these solutions [21]–[25], [30], [39] perform voltage equalization (also referred to as "virtual parallel operation" in some literature). That is, instead of locating the precise MPP, these solutions are striving to equalize all submodule voltages, so each submodule does not really operate at MPP during voltage equalization. Rather than performing *true* MPPT, voltage equalization only performs *near* MPPT. Although true DPP MPPT has been proposed for large-scale PV systems with central inverters [19], [20], [26]–[28], [34], [41], the solutions proposed to date have relatively high complexity in terms of control method or circuit implementation, while solutions more suited for microinverters have not yet been explored. Nowadays, microinverters are the preferred solution for residential PV installations. In residential PV applications, partial shading

and other types of mismatch can be more frequent and severe. Therefore, submodule-level compensation is even more crucial, yet not fully addressed in microinverter systems.

In this paper, we propose a solution that seamlessly combines commercial microinverters with DPP converters to address submodule mismatch with minimal additional hardware cost and no change to the existing microinverter design. The key contribution of this paper is the development of a control scheme to interface DPP converters with a microinverter to perform submodule-level MPPT. The DPP control algorithm is designed to be independent of the microinverter control such that no modification to the existing microinverter design is required. Additionally, we discuss the tradeoff between true MPPT and the voltage equalization in terms of control overhead and tracking efficiency, and perform both simulations and experiments to illustrate their differences. We identify the system impact of real-world challenges, such as the double line frequency ripple caused by the microinverter and propose solutions such as the digitally assisted windowed current measurement to address these challenges. Moreover, we design a DPP converter that achieves high efficiency and substantial hardware miniaturization to the point where it can fit into a PV junction box. A DPP converter hardware prototype has been built to work with a commercial off-the-shelf microinverter, and both laboratory and field tests have been performed to prove the concept.

The remainder of this paper is organized as follows: Section II discusses the control of DPP converters and their interaction with the microinverter. The tradeoff between true MPPT and voltage equalization is also analyzed. Section III presents the design of the DPP converters and the digitally assisted windowed current sensing technique. Section IV provides the experimental results of the DPP converters tested with a commercial microinverter. Finally, Section V concludes this paper.

II. Control

This section provides an overview on the operation of the merged system of the microinverter and DPP converters as well as detailed analyses on its control. The control problem of achieving submodule-level MPPT with DPP converters in a microinverter system is formulated. Simulation based on real PV module data is performed to illustrate the improvement on energy capture. True MPPT operation and voltage equalization are compared. In particular, the benefit of implementing true MPPT over voltage equalization is quantified while the tradeoff is analyzed.

A. System Overview

We propose merging DPP converters into a microinverter system, as shown in Fig. 3, to improve its energy capture. The DPP converters can be implemented as bidirectional buck–boost converters (see Section III for implementation details). By changing the duty ratio accordingly, each DPP converter can enforce a desired voltage ratio between neighboring submodules. Together with the microinverter that enforces certain module voltage (sum of the three submodule voltages), under proper control, the DPP converters can adjust the voltage of each submodule toward its individual maximum power point voltage. Therefore, each PV submodule can operate at its maximum power point. Meanwhile, current that is common to all submodules flows directly through the microinverter series connection, while the DPP converters shuffle the current mismatches between adjacent submodules, i.e., the DPP converters provide a path for the differential currents. A mathematical proof that a DPP system, as shown in Fig. 3, is capable of true MPPT operation can be derived, and interested readers are referred to [40] for details.

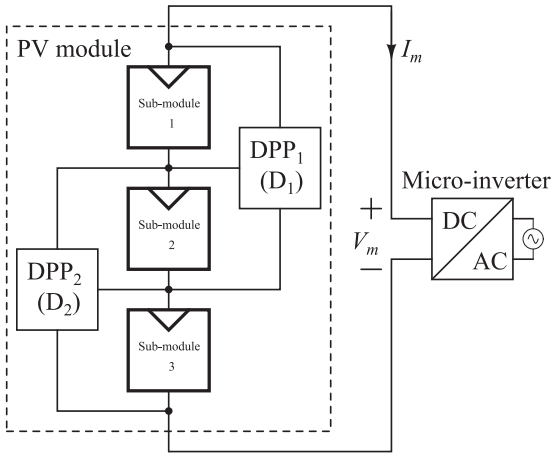

Fig. 3. Schematic of the proposed microinverter system with DPP converters.

B. Control Problem Formulation

To design a proper control method for MPPT in this DPP system, first consider the operation of the microinverter. Most existing designs of commercial microinverters operate a module-level MPPT based on a voltage-referenced perturb and observe (P&O) algorithm, in which the microinverter temporarily enforces a certain PV module voltage V_m. Therefore, the microinverter can be considered a controlled voltage source. When the microinverter executes its P&O algorithm, it perturbs the module voltage periodically, observes the resulting PV module current, and calculates the change in the PV module output power to decide the direction of the next voltage perturbation. While it may appear at first glance that significant coupling exists between the operation of the microinverter and that of the DPP converters, this is not the case in practice. As will be shown in Section III, the DPP converters can be designed to operate at a high switching frequency (on the order of hundreds of kilohertz) and, thus, have a much smaller time constant than the perturbation interval of V_m (typically on the order of tens of hertz). For the DPP converters, the PV module voltage can be considered temporarily fixed by the microinverter at any given time during the P&O interval. Since the power output of the PV module is

$$P_m = V_m \times I_m, \tag{1}$$

given a temporarily fixed module voltage, the power output of the PV module is maximized when the module current I_m is maximized, regardless of details of the mismatch between submodules. With a fixed V_m, for given environmental

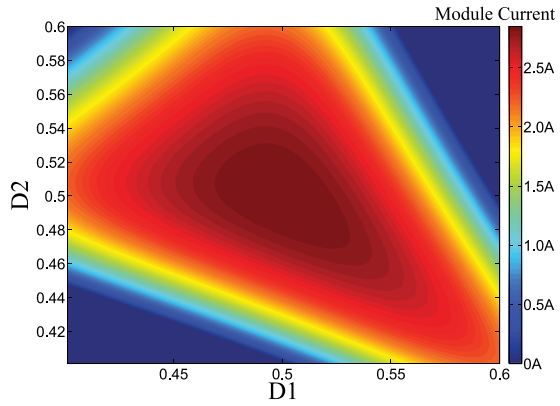

Fig. 4. Visualization of the module current I_m as a function of DPP converter duty ratios $(D1, D2)$ with a normalized irradiance profile of 100%, 80%, 50% on three PV submodules and module voltage fixed at 30 V.

conditions (irradiance, temperature, etc.), the module current is only a function of the duty ratios of the two DPP converters, (D_1, D_2), i.e.,

$$I_m = f(D_1, D_2). \tag{2}$$

Therefore, the control problem for the DPP converters can be simplified to

$$\begin{aligned} &\text{maximize} \quad I_m(D_1, D_2), \\ &\text{subject to} \quad V_1 + V_2 + V_3 = V_m. \end{aligned} \tag{3}$$

As an example, Fig. 4 shows a simulation result that visualizes I_m as a function of (D_1, D_2), given a certain V_m, in a contour plot with a normalized irradiance profile of 100%, 80%, 50% on the three submodules. It is clear from Fig. 4 that this function $I_m = f(D_1, D_2)$ has only one maximum. It is also easy to see that, similar to the control algorithm demonstrated in [26], the DPP converters can maximize the module current I_m by a DPP converter P&O algorithm that perturbs the duty ratios (D_1, D_2) and observes the change in I_m as illustrated by Fig. 5. Note that both DPP converters directly read and execute the duty ratio value from this control loop. The discrepancy in duty ratio and actual voltage conversion ratio due to converter nonideality has already been compensated in the MPPT control loop, so no lower level local control for DPP is required. The DPP converter P&O algorithm is implemented in a relatively fast control loop, while the original microinverter P&O algorithm is implemented in a relatively slow control loop. These two control loops operate independently from each other simultaneously to maximize the power of all submodules. The proposed control method is similar to the classical cascade control [43] with the small distinction that the former is a discrete P&O algorithm, while the latter is a continuous error-based PID control. The design of classical cascade control uses a rule-of-thumb approach and generally consider that the response time of the inner loop should be at least four times smaller than the outer control loop. In the prototype developed here, the fast loop was designed to be always at least ten times faster than the slow loop for adequate safety margins. As long as the fast control loop is at least 10 to 20 times faster than the slow control loop, the module voltage V_m can be considered temporarily fixed for DPP converters. Under these conditions, the proposed DPP control algorithm is capable of submodule MPPT as analyzed above.

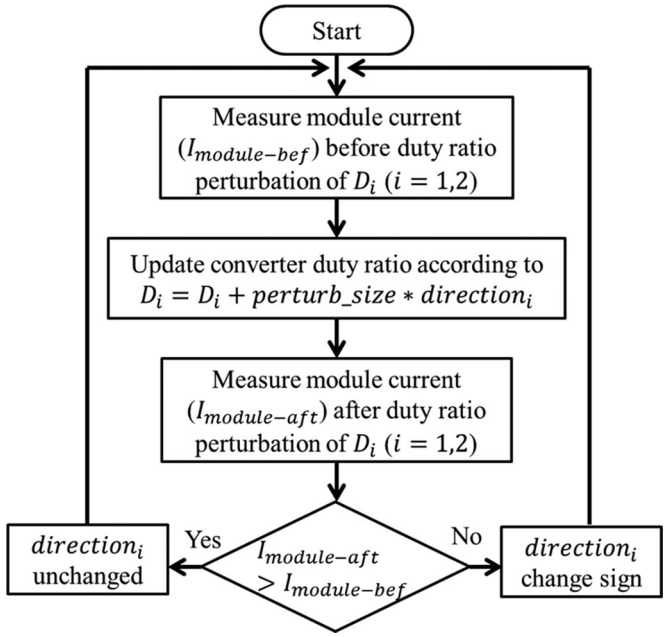

Fig. 5. Flowchart of the control algorithm for DPP converters.

Moreover, as can be seen from Fig. 4 and other similar simulations, when the mismatch between submodules is not severe, the optimal operating point of DPP is often very close to $(D_1, D_2) = (0.5, 0.5)$. This is because, within certain mismatch level, the maximum power point voltage of submodules does not change much with irradiance [23] (a detailed example is presented in Section II-C). Therefore, the control of DPP converters can be simplified: instead of DPP P&O, all DPP converters can simply run at a fixed 0.5 duty ratio with open-loop control to perform a *near* MPPT operation. This operation essentially equalizes all submodule voltages, and is capable of compensating for most of the potential power loss due to mismatch [21], [23], [30].

C. Comparison Between DPP and Bypass Diodes

To quantify the power yield improvement with DPP (both voltage equalization and true MPPT) over the conventional bypass diode solution, the following simulation has been performed: the *P–V* characteristics of the three submodules of a PV module (Sunmodule SW 235 Poly) are *measured* under different irradiance conditions (the experimental method to perform these measurements can be found in [44]); one example of the submodule *P–V* curves for a particular irradiance condition (100%, 40%, 20% normalized irradiance) is shown in Fig. 6; the measured submodule data are used to calculate the *P–V* curve of the entire module seen by the microinverter, with either bypass diode or DPP. Fig. 7 presents the module *P–V* curve corresponding to the condition of Fig. 6. Fig. 7 illustrates that DPP converters, with either control method, achieve significant improvement (more than 1.5 times for this

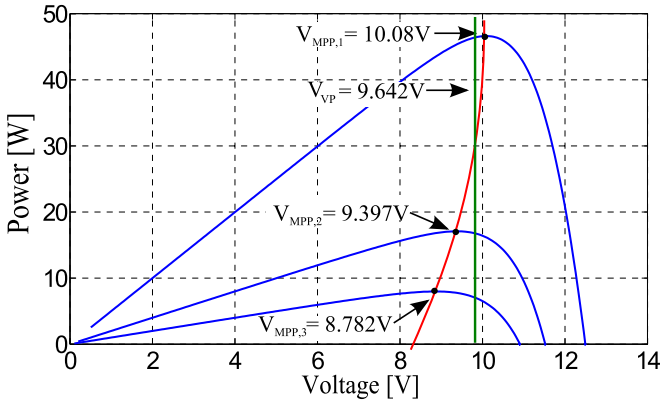

Fig. 6. *P–V* curve of each submodule in a condition of (100%, 40%, 20%) normalized irradiance. Each submodule operates at its own maximum power point voltage under true MPPT, while they all operate at V_{VP} under voltage equalization.

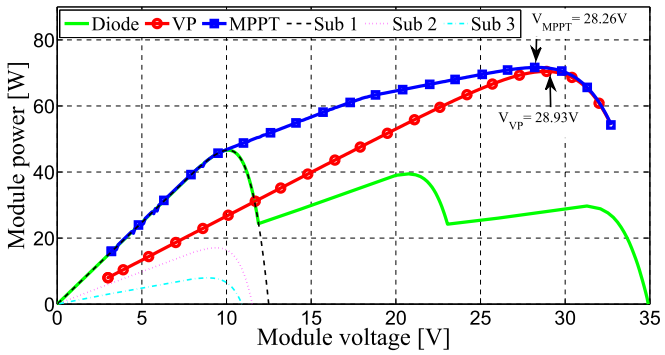

Fig. 7. *P–V* curve of the PV module with diode, DPP running voltage equalization and DPP running true MPPT in an irradiance condition corresponding to Fig. 6. The submodule *P–V* curves in Fig. 6 are plotted as well for reference.

particular condition) over bypass diode compensation in terms of maximum power output. The DPP converters also eliminate the local maxima caused by the conduction of bypass diodes, so the module *P–V* curve is smooth with only one maximum. This feature greatly facilitates the tracking operation of the microinverter (as will be shown by the experiment in Section IV).

D. Tradeoff Between Voltage Equalization and True MPPT

While true MPPT control gives the theoretical optimal power output, the simpler voltage equalization reduces the control overhead. The tradeoff between MPPT precision and the control overhead is fundamental and requires careful design consideration.

Figs. 6 and 7 illustrate the optimal module voltage for voltage equalization and true MPPT on the submodule level and the module level, respectively. Together with Fig. 4, it is easy to see that the operating point of voltage equalization $(V_{\mathrm{VP}}, 0.5, 0.5)$ is close to that of true MPPT, $(V_{\mathrm{MPPT}}, D_{1,\mathrm{MPPT}}, D_{2,\mathrm{MPPT}})$, while voltage equalization extracts slightly less power than true MPPT. To further quantify the power difference between voltage equalization and true MPPT in all irradiance conditions, the

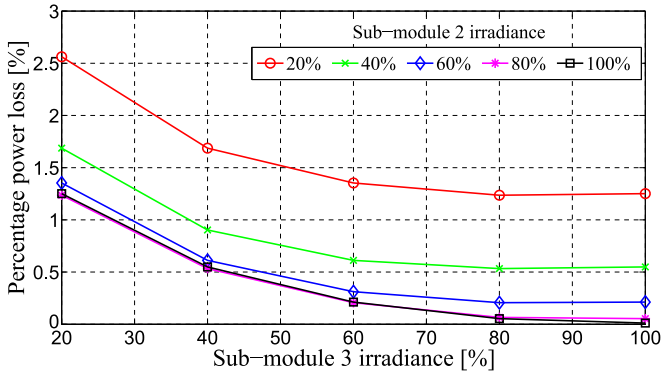

Fig. 8. Percentage power loss due to voltage equalization operation instead of true MPPT for different irradiance conditions. Submodule 1 is fixed at 100% normalized irradiance, submodule 2 is fixed at 20% , 40%, 60%, 80% and 100% normalized irradiance, and submodule 3 is sweep from 20% normalized irradiance to 100% normalized irradiance.

percentage power loss due to voltage equalization, defined as

$$\tau = 1 - \frac{P_{\mathrm{VP,max}}}{P_{\mathrm{MPPT,max}}},$$

is plotted in Fig. 8.

Although from Fig. 8, it seems that the potential power loss of voltage equalization is not significant unless the mismatch is very severe, it should be noted that severe mismatch does happen quite frequently in residential installations. According to the study in [45], shading 10% of the solar module can result in more than 50% power loss. Fig. 9 shows the measured *P–V* curve of a PV module (Sunmodule SW 235 Poly) with only a small part of a submodule shaded, and significant power mismatch can be observed. Moreover, while the analysis in Fig. 8 considers the best-case scenario of newly installed well-binned [46] PV modules with no thermal gradients, factors such as nonuniform ageing [47], temperature difference, less stringently binned modules (to reduce manufacturing cost) may further increase the mismatch and, under certain circumstances, justify the use of true MPPT [28].

On the other hand, voltage equalization significantly reduces the control overhead while maintaining good tracking efficiency. DPP converters can simply run with open-loop control, requiring no real-time sensing or communication. In comparison, to perform true MPPT, the module current I_m has to be measured. Additional hardware is required if no modification at all is allowed on the microconverter. Otherwise, since the microinverter needs to measure the module current I_m for its own operation, and the microinverter is often installed immediately on the backside of the PV module and, thus, physically close and accessible to the DPP converters, the DPP converters can share the same current sensing device (such as a current sensing resistor) with the microinverter, eliminating the loss introduced by extra current sensing. However, a separate amplification and filtering circuit may be needed for the DPP converters, since they need to sense the current change faster than the microinverter owing to the need for a faster tracking loop. In the ideal case, the DPP converters can be merged into the microinverter circuit board and share the same control unit, since the control unit typically

(a)

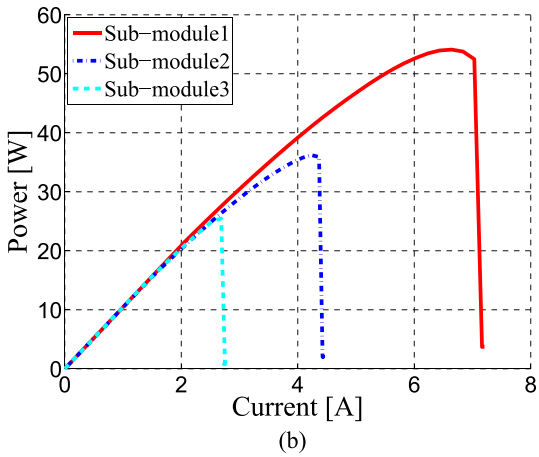

(b)

Fig. 9. Partial shading setup and the corresponding submodule *P–I* curves. (a) Shading scenario. (b) Submodule *P–V* curves.

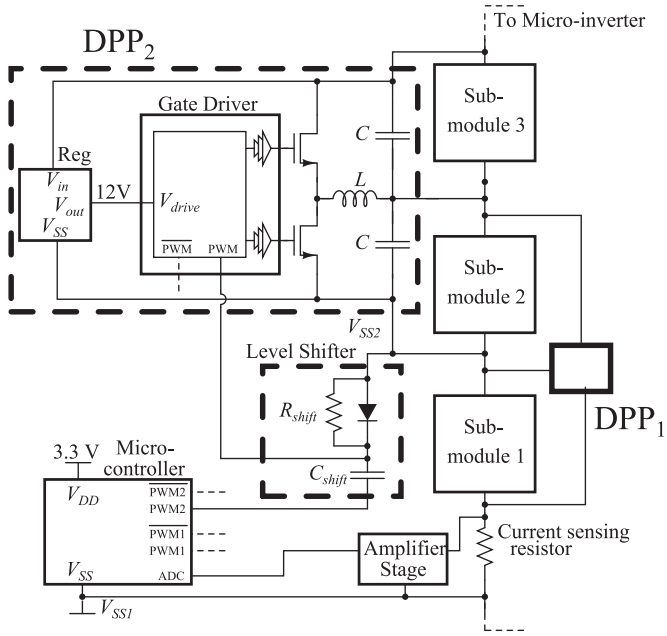

Fig. 10. Schematic of the DPP converter prototype design.

TABLE II
MAIN COMPONENT LIST

Device	Model	Value	Manufacturer
Microcontroller	STM32F105		STMicroelectronics
MOSFET	CSD18504Q5A		Texas Instruments
Linear Regulator	KA78L12AMTF		Fairchild
L	SER1360-103KL	10 μH	Coilcraft
C	TMK212BBJ106KG-T	10 μF×4	Taiyo Yuden
D_{shift}	1SS416CT(TPL3)		Toshiba
C_{shift}	0402	1 nF	
R_{shift}	0402	40 kΩ	
Amplifier	LMP8602		Texas Instruments
Amplifier	OPA188		Texas Instruments

has enough resources to control the DPP converters as well. In this way, DPP can be incorporated into the microinverter system with minimal additional hardware cost.

Based on the above analysis, the choice between voltage equalization and true MPPT typically depends on the application requirement. If DPP can be designed as part of the microinverter, true MPPT operations can be implemented with low additional cost. For a standalone implementation of DPP, voltage equalization is often the more feasible solution. Since microinverter design is not in the scope of this paper, for the rest of this paper, we mainly focus on the standalone implementation of DPP converters.

III. DPP Converter Design

In this section, the goal of the DPP hardware design is specified and a standalone implementation of the DPP converters is presented. In addition, the challenge associated with module current sensing is analyzed and a solution using a digitally assisted windowed sensing technique is presented.

A. Hardware Design Goal

Since the DPP converters only process the differential power between submodules, the voltage and power ratings required for the DPP converters are relatively low. The low voltage rating enables the use of small, fast-switching transistors. Since the energy storage components in the converters (especially inductors) often dominate the circuit size, the use of a high switching frequency allows for significant size reduction of the DPP converters. A circuit size reduction that fits the DPP converters into the PV module junction box or into the microinverter chassis is highly desirable, since otherwise, the cost of a separate enclosure for the DPP converters will significantly add to the total system cost [48]. The goal of the hardware design is to build a converter that achieves these objectives.

B. DPP Hardware Design

With these design goals in mind, a DPP converter hardware prototype design is proposed. The circuit schematic is shown in Fig. 10 and component selection is summarized in Table II. Note that Fig. 10 only shows the details of DPP_2 (those of DPP_1

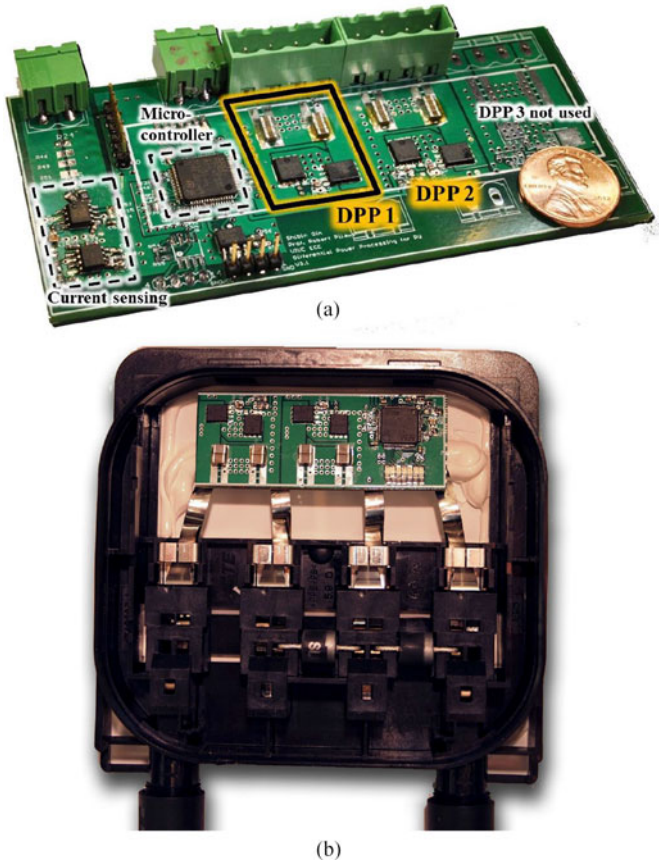

Fig. 11. Photograph of hardware prototype. (a) Complete hardware prototype (with a one-cent coin for scale). The circuit board incorporates three DPP converters for future development, while only two DPP converters are used in this paper. (b) Photograph of the hardware prototype fitting into a junction box.

are identical and thus omitted). In this paper, DPP converters are implemented as bidirectional synchronous buck–boost converters switching at 300 kHz. A microcontroller, a current sensing circuit, and a communication interface are also incorporated into this design to implement the control algorithm of the DPP converters and to facilitate data collection. An annotated photograph of the DPP converter prototype built based on this design is shown in Fig. 11(a) (inductors are located on the back side of the PCB). Note the small size of each DPP converter, which will consume little additional circuit board space if merged with the microinverter, or easily fit into a PV module junction box if implemented as a standalone circuit as shown in Fig. 11(b). Note that the main converter circuit as well as the auxiliary circuits have relatively low circuit complexity. More importantly, the proposed solution is an "add-on" circuit to the microinverter system. No modification to the original microinverter system is required. As shown in Figs. 10 and 11(b), DPP converters can be simply attached to the PV string in the junction box. In comparison, as shown in Fig. 1(a), the original series wiring of the PV module has to be cut to install submodule dc optimizers, making them incompatible with existing PV module manufacturing steps. Moreover, the microinverter design and connection do not need to be changed for the proposed DPP system. In summary, the DPP circuit implementation itself has low complexity and does not add considerable complexity to the overall system.

TABLE III
HARDWARE PROTOTYPE SPECIFICATIONS

Submodule Voltage Range	5–20 V
Power Rating (each converter)	60 W
Switching Frequency	300 kHz
Converter Peak Efficiency	95%
Weight	25 g
Volume	17.29 cm^3

The main converter specifications are presented in Table III. In a typical 250-W PV module, the worst case power that one DPP converter needs to process is approximately 55 W, which corresponds to the case when one submodule is fully illuminated and the other two fully shaded. In this paper, the converter prototype is rated at 60 W. A control method similar to the one presented in [49] can be developed to further reduce the power rating of each converter by trading off the MPPT performance versus power rating. The maximum converter power is bounded by the local converter control scheme to a value lower than the worst-case power rating, but the converter can only perform near MPPT when the power reaches the new converter limit. Such control method will further reduce the size and power loss of the DPP converters, while not impacting the overall performance of the system too much since the worst-case scenario does not happen frequently.

C. Windowed Current Measurement

A challenge of implementing the proposed control algorithm for true MPPT is how to precisely sense the small current change resulting from the converter duty ratio perturbations. The conventional solution is to use a small current sensing resistor and an amplifier to convert the module current linearly into a voltage signal and feed it to the microcontroller ADC. In this application, the module current typically ranges from 1 up to 8 A depending on the irradiance, so the gain ratio from the current to the voltage signal has to be limited to avoid saturating the ADC. At the same time, the small current change due to DPP perturbation can be as low as tens of milliampere, which, after converted to a voltage signal with the same gain ratio, is typically smaller than the ADC resolution of a typical low-cost microcontroller. On the other hand, the requirement on the effective ADC speed and accuracy is not strict in this application, which allows for the opportunity to improve the ADC with existing resources on a typical low-cost microcontroller.

To this end, it is observed that, since the P&O algorithm only uses the relative change between two measurements, the large dc value can be subtracted from the signal beforehand using digital feedback such that the small change can be further amplified. Therefore, the digitally assisted windowed sensing technique has been adopted from [50] to implement the current sensing circuitry as shown in Fig. 12. The first stage uses a conventional current sensing method: The module current signal is converted into a voltage signal by a 5-mΩ current sensing resistor and scaled up linearly by an amplifier with a fixed gain of 50. For a module current change of 10 mA, the output voltage signal $v_{\rm sense}$ only changes 2.5 mV, which is too small to be effectively captured by the microcontroller's ADC. However, any attempt to

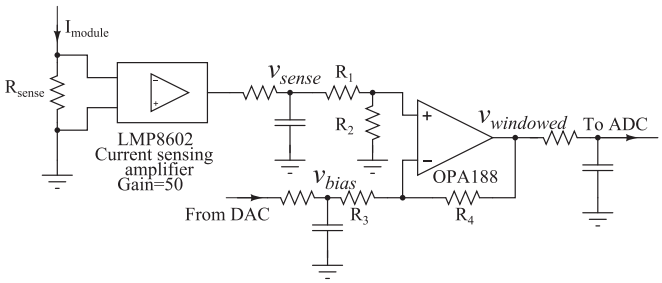

Fig. 12. Schematic of the current sensing circuity using a measurement windowing technique.

further increase the gain of this circuit will saturate the amplifier output and the ADC since a large average value is also present in the module current. To decouple the relative change and absolute value of the signal and further amplify the relative change, the voltage signal $v_{\rm sense}$ is passed to a voltage subtractor (differential amplifier) stage. A voltage reference $v_{\rm bias}$ that is slightly smaller than $v_{\rm sense}$ is subtracted from $v_{\rm sense}$, and the resulting small difference can then be further amplified by the differential amplifier to get $v_{\rm windowed}$, i.e.,

$$v_{\rm windowed} = \frac{R_2}{R_1}(v_{\rm sense} - v_{\rm bias}), \tag{4}$$

$$\text{given that} \quad R_1 = R_3, \qquad R_2 = R_4. \tag{5}$$

In this design, we select $R_1 = R_3 = 1\,\text{k}\Omega$, $R_2 = R_4 = 50\,\text{k}\Omega$, so a 10 mA change in module current results in a 5 mV change in $v_{\rm sense}$ and eventually a 250 mV change in $v_{\rm windowed}$, which is large enough to be sensed by the microcontroller's ADC. The signal $v_{\rm bias}$ is provided by the microcontroller's DAC output and can be adjusted by the microcontroller to make sure that it is always slightly smaller than $v_{\rm sense}$ to avoid saturating the differential amplifier output or the ADC. In our implementation, before a DPP perturbation, the microcontroller will adjust $v_{\rm bias}$ such that $v_{\rm windowed}$ is within 40% to 60% of the ADC range, fix the value of $v_{\rm bias}$, then trigger the DPP perturbation, and observe the change in $v_{\rm windowed}$ (the change of $v_{\rm windowed}$ can even saturate the ADC; the MPPT algorithm will not be affected since it only needs the direction of the change instead of the exact value of $v_{\rm windowed}$). The *RC* filter in the circuit is carefully selected such that the switching ripple of the converters will not affect the measurements.

IV. Experimental Results

A. Experimental Setup

We have developed an experimental setup as shown in Fig. 13 to verify the effectiveness of the proposed method and to demonstrate the ability of the DPP converters to work with a commercial off-the-shelf microinverter. In the setup, a Sunmodule SW 235 Poly PV module consisting of three submodules was used. The PV module was connected to the dc side of a Pantheon II microinverter from SolarBridge Technologies. The P&O algorithm of the microinverter was slowed down to about 1 Hz for data capture purposes. A 112-AMX ac power supply that generated a 220-V sinusoidal voltage to emulate the grid was

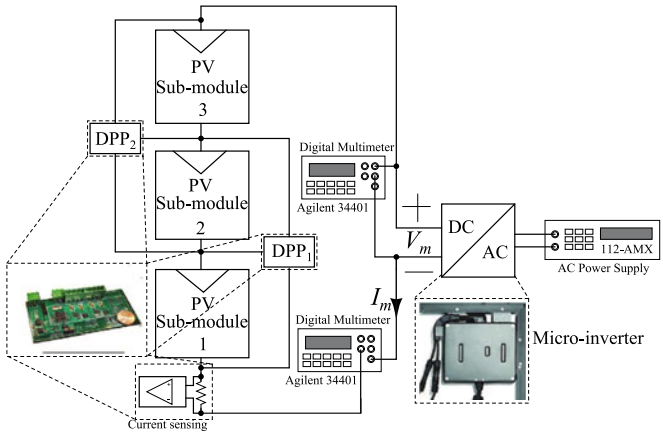

Fig. 13. Experimental setup.

connected to the ac side. The microinverter, together with the ac power supply, also powered a 370-W load consisting of four light bulbs that were also connected to the ac side. Two Agilent 34401A multimeters were used to measure the PV module voltage and current on the dc side. During the entire experiment, the microinverter was set to operate autonomously.

B. Indoor Experiments

Instead of testing the experimental setup in an outdoor environment directly, where the environmental factors are uncontrollable and constantly changing, we conducted the initial stage of our experiments indoors in a more controllable and repeatable manner. The PV emulation technique in [44] was used: each submodule was connected in parallel with a HP6634A dc power supply (omitted in Fig. 13) in current-limited mode; the power supply current replicates the photogenerated current to emulate the effect of sunlight illumination; the current-limit value (i.e., the amount of current sourced by each dc power supply) determines the intensity of the emulated irradiance on each submodule. In the experiment, mismatch between submodules (e.g., an irradiance profile of 100%, 50%, 100% normalized values) was emulated.

For the first part of the experiment, an HP6060B electronic load was connected to the PV module to perform a dc voltage sweep to characterize the *P–V* curve of the PV module with and without the DPP converters running. The resulting *P–V* curve is plotted in Fig. 14(a), which corresponds to the simulation result shown in Fig. 7. The low-voltage range (below 15 V) of dc sweep was not performed for DPP-compensated modules in the experiment because the gate driver of each DPP converter draws power from its corresponding submodule, and the voltage on each submodule is too low to turn the DPP converter on when the entire module voltage is below 15 V. The maximum power of the *P–V* curve with each compensation method is listed and compared with simulation result in Table IV. Note that for diode compensation, the bypass diode of the weak submodule conducted and created a nonconcave module *P–V* curve with local maxima, which can trap the MPPT operation of the microinverter; its actual power output with diode compensation is much smaller than simulated value because of the power loss

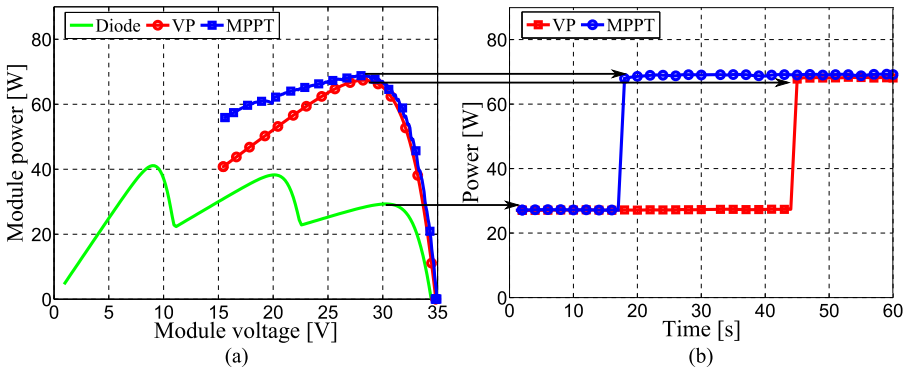

Fig. 14. Indoor experimental results. (a) PV module power versus module voltage (dc sweep with electronic load). (b) PV module power versus time (full system operation with microinverter).

TABLE IV
EXPERIMENTAL RESULT SUMMARY AND COMPARISON

Experiment	Specifications	Measured	Simulated
dc sweep	Bypass diode maximum power [W]	41.10	46.61
	MPPT maximum power [W]	68.79	71.16
	Voltage equalization maximum power [W]	67.40	70.46
Microinverter	Bypass diode maximum power [W]	27.18	-
	MPPT maximum power [W]	69.11	-
	Voltage equalization maximum power [W]	68.32	-

from diode forward voltage drop. With the DPP converters running, the mismatch was compensated by the DPP converters without turning ON the bypass diodes, and the resulting *P–V* curve was concave. Note that due to limited dc sweep resolution, limited DPP duty ratio resolution and converter power loss, the measured maximum power is less than the simulated value (which represents the absolute best case with ideal converter and very fine tracking resolution). Nevertheless, using DPP converters with either control method achieves more than 1.6 times improvement over conventional diode compensation in the experiment.

For the second part of the experiment, the PV module under the same irradiance condition was tested with the microinverter. Fig. 14(b) shows the real-time power from the PV module into the dc side of the microinverter. The DPP converters were initially turned OFF, so the PV module has only diode compensation. Then, the DPP converters were turned ON half-way through the test to show the improvement in power output. For one test, the DPP converters running voltage equalization were turned ON at $t = 43$ s; for another test, the DPP converters running true MPPT were turned ON at $t = 17$ s. Without the DPP converters running, the microinverter was trapped by a local maximum as expected, incurring even more power losses. Once the DPP converters were turned ON, they smoothed the module *P–V* curve. The microinverter quickly converged to the new operating point and the power losses were recovered.

A challenge associated with interfacing DPP converters with a microinverter is the double line frequency ripple created by the microinverter. This problem is very common in single-phase inverters: The microinverter dc side has constant dc power input, while the ac side outputs ac power of twice the line frequency; energy has to be stored temporarily when the instantaneous power output is different from the constant power input; this storage is typically implemented by charging and discharging a dc-link capacitor or ripple port, resulting in terminal current and voltage ripples [51]. This ripple might be on the same order as, or even larger than the current change caused by the DPP converter perturbation. The DPP converter MPPT operation would thus be interfered with, resulting in compromised tracking performance. In this paper, we implemented the filter of the current sensing circuitry with low enough cutoff frequency, and also averaged the ADC readings over the time period of double line frequency to eliminate the effect of this ripple so that the DPP can perform MPPT. However, this also limits the control bandwidth of DPP MPPT operation below the double line frequency. Even so, the performance of DPP compensation is lower bounded by the voltage equalization, which still provides significant improvement over the conventional diode compensation.

C. Field Experiments

While the indoor experiments illustrate the static tracking performance of DPP, to further verify the effectiveness of DPP in a dynamic real-world environment, the same experimental setup in Fig. 13 was tested outdoors under real sunlight illumination. The shading pattern used is the same as shown in Fig. 9(a). As the sun moves throughout the day, the shadow cast by the cylinder moves as well, representing a moving shading pattern, simultaneously. The leaves represent a fixed shading pattern, yielding an overall shading pattern containing both constant and time-varying mismatch. For comparison purposes, the test was set up such that for every 60 s, the DPP converters were turned ON for 30 s and OFF for the other 30 s (leaving the module with only the conventional diode compensation). The microinverter was connected to the PV module and performed its module-level MPPT all the time. The module power at the end of each 30 s was recorded to represent the corresponding module power output with and without DPP converters for that minute. An example of the measured PV module power over time in a partially cloudy day is shown in Fig. 15 (note that the controller only ran voltage equalization in this field test). During this 1-h period, DPP converters always improve the module

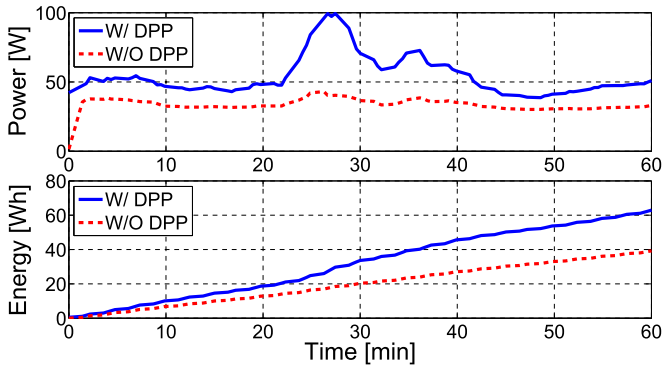

Fig. 15. PV module power output and accumulative energy output with and without DPP converters over a 1-h period during the field test.

power output, and the accumulative energy yield is about 1.6 times higher than diode compensation. The field test data further demonstrates the ability of DPP converters to enable significant power output improvement in a real-world environment.

V. Conclusion

In this paper, we addressed the problem of submodule mismatch in a microinverter system by combining the microinverter with DPP converters. Without any modification to the existing microinverter hardware, DPP converters can be integrated into the system with the proposed DPP converter hardware design and the control scheme to perform submodule-level maximum power point tracking. Experiments with a commercial off-the-shelf microinverter were conducted and the improvement in performance with DPP converters was experimentally confirmed.

Acknowledgment

The authors would like to thank J. Ehlmann of Solarbridge Technologies for his help with the experimental setup.

References

[1] K. Kim and P. Krein, "Hot spotting and second breakdown effects on reverse I–V characteristics for mono-crystalline Si photovoltaics," in *Proc. IEEE Energy Convers. Congr. Expo.*, Sep. 2013, pp. 1007–1014.

[2] K. A. Kim, P. T. Krein, G.-S. Seo, and B.-H. Cho, "Photovoltaic ac parameter characterization for dynamic partial shading and hot spot detection," in *Proc. IEEE 28th Annu. Appl. Power Electron. Conf. Expo.*, Mar. 2013, pp. 109–115.

[3] G. R. Walker and P. C. Sernia, "Cascaded dc-dc converter connection of photovoltaic modules," *IEEE Trans. Power Electron.*, vol. 19, no. 4, pp. 1130–1139, Jul. 2004.

[4] N. Femia, G. Lisi, G. Petrone, G. Spagnuolo, and M. Vitelli, "Distributed maximum power point tracking of photovoltaic arrays: Novel approach and system analysis," *IEEE Trans. Ind. Electron.*, vol. 55, no. 7, pp. 2610–2621, Jul. 2008.

[5] L. Linares, R. Erickson, S. MacAlpine, and M. Brandemuehl, "Improved energy capture in series string photovoltaics via smart distributed power electronics," in *Proc. Appl. Power Electron. Conf. Expo.*, 2009, pp. 904–910.

[6] Q. Li and P. Wolfs, "A review of the single phase photovoltaic module integrated converter topologies with three different dc link configurations," *IEEE Trans. Power Electron.*, vol. 23, no. 3, pp. 1320–1333, May 2008.

[7] R. Erickson and A. Rogers, "A microinverter for building-integrated photovoltaics," in *Proc. Appl. Power Electron. Conf. Expo.*, 2009, pp. 911–917.

[8] A. Trubitsyn, B. Pierquet, A. Hayman, G. Gamache, C. Sullivan, and D. Perreault, "High-efficiency inverter for photovoltaic applications," in *Proc. Energy Convers. Congr. Expo.*, 2010, pp. 2803–2810.

[9] R. Pilawa-Podgurski and D. Perreault, "Submodule integrated distributed maximum power point tracking for solar photovoltaic applications," *IEEE Trans. Power Electron.*, vol. 28, no. 6, pp. 2957–2967, Jun. 2013.

[10] Y.-S. Lee and M.-W. Cheng, "Intelligent control battery equalization for series connected lithium-ion battery strings," *IEEE Trans. Ind. Electron.*, vol. 52, no. 5, pp. 1297–1307, Oct. 2005.

[11] C. Pascual and P. Krein, "Switched capacitor system for automatic series battery equalization," in *Proc. 12th Annu. Appl. Power Electron. Conf. Expo.*, Feb. 1997, vol. 2, pp. 848–854.

[12] J. McClurg, Y. Zhang, J. Wheeler, and R. Pilawa-Podgurski, "Re-thinking data center power delivery: Regulating series-connected voltage domains in software," in *Proc. IEEE Power Energy Conf. Illinois*, Feb. 2013, pp. 147–154.

[13] J. McClurg, R. Pilawa-Podgurski, and P. Shenoy, "A series-stacked architecture for high-efficiency data center power delivery," in *Proc. IEEE Energy Convers. Congr. Expo.*, Sep. 2014, pp. 170–177.

[14] E. Candan, P. Shenoy, and R. Pilawa-Podgurski, "A series-stacked power delivery architecture with isolated differential power conversion for data centers," in *Proc. IEEE 36th Int. Telecommun. Energy Conf.*, Sep. 2014, pp. 1–8.

[15] P. Shenoy, S. Zhang, R. Abdallah, P. Krein, and N. Shanbhag, "Overcoming the power wall: Connecting voltage domains in series," in *Proc. Int. Conf. Energy Aware Comput.*, Nov. 2011, pp. 1–6.

[16] S. Zhang, J. Tu, N. Shanbhag, and P. Krein, "A 0.79 pj/k-gate, 83% unified core and voltage regulator architecture for sub/near-threshold operation in 130 nm cmos," *IEEE J. Solid-State Circuits*, vol. 49, no. 11, pp. 2644–2657, Nov. 2014.

[17] C. Schaef and J. T. Stauth, "A multilevel VR implementation and MIMO control scheme for vertically-stacked microprocessor cores," in *Proc. IEEE Appl. Power Electron. Conf. Expo.*, Mar. 2015, pp. 2090–2096.

[18] C. Schaef and J. T. Stauth, "Efficient voltage regulation for microprocessor cores stacked in vertical voltage domains," *IEEE Trans. Power Electron.*, vol. pp, no. 99, pp. 1–1, Apr. 2015.

[19] T. Shimizu, M. Hirakata, T. Kamezawa, and H. Watanabe, "Generation control circuit for photovoltaic modules," *IEEE Trans. Power Electron.*, vol. 16, no. 3, pp. 293–300, May 2001.

[20] T. Shimizu, O. Hashimoto, and G. Kimura, "A novel high-performance utility-interactive photovoltaic inverter system," *IEEE Trans. Power Electron.*, vol. 18, no. 2, pp. 704–711, Mar. 2003.

[21] C. Olalla, D. Clement, M. Rodriguez, and D. Maksimovic, "Architectures and control of submodule integrated dc-dc converters for photovoltaic applications," *IEEE Trans. Power Electron.*, vol. 28, no. 6, pp. 2980–2997, Jun. 2013.

[22] C. Olalla, C. Deline, and D. Maksimovic, "Modeling and simulation of conventionally wired photovoltaic systems based on differential power processing submic-enhanced PV modules," in *Proc. IEEE 15th Workshop Control Model. Power Electron.*, Jun. 2014, pp. 1–9.

[23] J. Stauth, M. Seeman, and K. Kesarwani, "Resonant switched-capacitor converters for sub-module distributed photovoltaic power management," *IEEE Trans. Power Electron.*, vol. 28, no. 3, pp. 1189–1198, Mar. 2013.

[24] H. Bergveld, D. Buthker, C. Castello, T. Doorn, A. de Jong, R. van Otten, and K. de Waal, "Module-level dc/dc conversion for photovoltaic systems: The delta-conversion concept," *IEEE Trans. Power Electron.*, vol. 28, no. 4, pp. 2005–2013, Apr. 2013.

[25] J. Du, R. Xu, X. Chen, Y. Li, and J. Wu, "A novel solar panel optimizer with self-compensation for partial shadow condition," in *Proc. IEEE 28th Annu. Appl. Power Electron. Conf. Expo.*, Mar. 2013, pp. 92–96.

[26] S. Qin and R. C. Pilawa-Podgurski, "Sub-module differential power processing for photovoltaic applications," in *Proc. Appl. Power Electron. Conf. Expo.*, 2013, pp. 101–108.

[27] S. Qin, S. Cady, A. Dominguez-Garcia, and R. Pilawa-Podgurski, "A distributed approach to MPPT for PV sub-module differential power processing," in *Proc. IEEE Energy Convers. Congr. Expo.*, Sep. 2013, pp. 2778–2785.

[28] S. Qin, S. Cady, A. Dominguez-Garcia, and R. Pilawa-Podgurski, "A distributed approach to maximum power point tracking for photovoltaic sub-module differential power processing," *IEEE Trans. Power Electron.*, vol. 30, no. 4, pp. 2024–2040, Apr. 2015.

[29] S. Qin, A. Morrison, and R. Pilawa-Podgurski, "Enhancing micro-inverter energy capture with sub-module differential power processing," in *Proc. IEEE 29th Annu. Appl. Power Electron. Conf. Expo.*, Mar. 2014, pp. 621–628.

[30] S. Poshtkouhi, A. Biswas, and O. Trescases, "dc-dc converter for high granularity, sub-string MPPT in photovoltaic applications using a virtual-parallel connection," in *Proc. Appl. Power Electron. Conf. Expo.*, 2012, pp. 86–92.
[31] M. Uno and A. Kukita, "Two-switch voltage equalizer using series-resonant inverter and voltage multiplier for partially-shaded series-connected photovoltaic modules," in *Proc. IEEE Energy Convers. Congr. Expo.*, Sep. 2013, pp. 1311–1318.
[32] M. Uno and A. Kukita, "Single-switch voltage equalizer using multi-stacked sepics for partially-shaded series-connected PV modules," in *Proc. 35th Int. Telecommun. Energy Conf. Smart Power Efficiency*, Oct. 2013, pp. 1–6.
[33] M. Uno and A. Kukita, "Two-switch voltage equalizer using an LLC resonant inverter and voltage multiplier for partially-shaded series-connected photovoltaic modules," *IEEE Trans. Ind. Appl.*, vol. 51, no. 2, pp. 1587–1601, Mar./Apr. 2015.
[34] R. Bell and R. Pilawa-Podgurski, "Asynchronous and distributed maximum power point tracking of series-connected photovoltaic sub-modules using differential power processing," in *Proc. IEEE 15th Workshop Control Model. Power Electron.*, Jun. 2014, pp. 1–8.
[35] A. Chang, A. Avestruz, and S. Leeb, "Capacitor-less photovoltaic cell-level power balancing using diffusion charge redistribution," *IEEE Trans. Power Electron.*, vol. 30, no. 2, pp. 537–546, Feb. 2015.
[36] M. Kasper, S. Herden, D. Bortis, and J. Kolar, "Impact of PV string shading conditions on panel voltage equalizing converters and optimization of a single converter system with overcurrent protection," in *Proc. 16th Eur. Conf. Power Electron. Appl.*, Aug. 2014, pp. 1–10.
[37] R. Sangwan, K. Kesarwani, and J. T. Stauth, "High-density power converters for sub-module photovoltaic power management," in *Proc. IEEE Energy Convers. Congr. Expo.*, Sep. 2014, pp. 3279–3286.
[38] K. Kim, P. Shenoy, and P. Krein, "Converter rating analysis for photovoltaic differential power processing systems," *IEEE Trans. Power Electron.*, vol. 30, no. 4, pp. 1987–1997, Apr. 2015.
[39] N. Pragallapati and V. Agarwal, "Flyback configuration based micro-inverter with distributed MPPT of partially shaded PV module and energy recovery scheme," in *Proc. IEEE 39th Photovoltaic Spec. Conf.*, Jun. 2013, pp. 2927–2931.
[40] P. Shenoy, K. Kim, B. Johnson, and P. Krein, "Differential power processing for increased energy production and reliability of photovoltaic systems," *IEEE Trans. Power Electron.*, vol. 28, no. 6, pp. 2968–2979, Jun. 2013.
[41] C. Schaef and J. T. Stauth, "Multilevel power-point-tracking for variable-conversion-ratio photovoltaic ladder converters," in *Proc. Workshop Control Model. Power Electron.*, 2013, pp. 1–7.
[42] C. Schaef and J. Stauth, "Multilevel power point tracking for partial power processing photovoltaic converters," *IEEE J. Emerging Sel. Topics Power Electron.*, vol. 2, no. 4, pp. 859–869, Dec. 2014.
[43] S. W. Mahoney, D. P. Mahoney, and B. Young, *A Real-Time Approach to Process Control*, 2nd ed. New York, NY, USA: Wiley, 2007.
[44] S. Qin, K. Kim, and R. Pilawa-Podgurski, "Laboratory emulation of a photovoltaic module for controllable insolation and realistic dynamic performance," in *Proc. Power Energy Conf. Illinois*, 2013, pp. 23–29.
[45] R. J. Muenster. (2009). Shade happens. *Renewableenergyworld.com*. [Online]. Available: http://www.renewableenergyworld.com/
[46] H. Field and A. Gabor, "Cell binning method analysis to minimize mismatch losses and performance variation in Si-based modules," in *Proc. Photovoltaic Spec. Conf.*, 2002, pp. 418–421.
[47] C. E. Chamberlin, M. A. Rocheleau, M. W. Marshall, A. M. Reis, N. T. Coleman, and P. Lehman, "Comparison of PV module performance before and after 11 and 20 years of field exposure," in *Proc. Photovoltaic Spec. Conf.*, 2011, pp. 101–105.
[48] C. Deline, B. Marion, J. Granata, and S. G. Sigifredo, "A performance and economic analysis of distributed power electronics in photovoltaic systems," Tech. Rep. NREL/TP-5200-50003, Jan. 2011.
[49] C. Olalla, D. Clement, B. S. Choi, and D. Maksimovic, "A branch and bound algorithm for high-granularity PV simulations with power limited submics," in *Proc. IEEE 14th Workshop Control Model. Power Electron.*, Jun. 2013, pp. 1–6.
[50] C. Barth and R. Pilawa-Podgurski, "Dithering digital ripple correlation control with digitally-assisted windowed sensing for solar photovoltaic MPPT," in *Proc. IEEE 29th Annu. Appl. Power Electron. Conf. Expo.*, Mar. 2014, pp. 1738–1746.
[51] P. Krein, R. Balog, and M. Mirjafari, "Minimum energy and capacitance requirements for single-phase inverters and rectifiers using a ripple port," *IEEE Trans. Power Electron.*, vol. 27, no. 11, pp. 4690–4698, Nov. 2012.

Shibin Qin received the B.E. degree in electrical engineering from the Huazhong University of Science and Technology, Wuhan, China, in 2012, and the M.S. degree in electrical engineering from the University of Illinois at Urbana-Champaign, Urbana, IL, USA, in 2014, where he is currently working toward the Ph.D. degree.

His research interests include high power density converters and photovoltaic applications.

Christopher B. Barth received the B.S. and M.S degrees in electrical and computer engineering from the University of Illinois at Urbana-Champaign, Urbana, IL, USA, in 2012 and 2014, respectively, where he is currently working toward the Ph.D. degree.

His research interests include high power density inverters for PV and motor drive applications.

Robert C.N. Pilawa-Podgurski received the dual B.S. degrees in physics and electrical engineering and computer science, the M.Eng. degree in electrical engineering and computer science, and the Ph.D. degree in electrical engineering, all from the Massachusetts Institute of Technology, Cambridge, MA, USA, in 2005, 2007, and 2012, respectively.

He is currently an Assistant Professor with the Electrical and Computer Engineering Department, University of Illinois, Urbana-Champaign, IL, USA, and is affiliated with the Power and Energy Systems group. He performs research in the area of power electronics. His research interests include renewable energy applications, energy harvesting, CMOS power management, and advanced control of power converters.

Dr. Pilawa-Podgurski received the Chorafas Award for outstanding MIT EECS Master's thesis, the Google Faculty Research Award in 2013, and the 2014 Richard M. Bass Outstanding Young Power Electronics Engineer Award of the IEEE Power Electronics Society, for outstanding contributions to the field of power electronics before the age of 35. In 2015, he received the Air Force Office of Scientific Research Young Investigator Award. He is an Associate Editor for the IEEE TRANSACTIONS ON POWER ELECTRONICS, and for the IEEE JOURNAL OF EMERGING AND SELECTED TOPICS IN POWER ELECTRONICS. He is the coauthor of four IEEE prize papers.